Grain boundary pinning and glassy dynamics in stripe phases

Denis Boyer*
School of Computational Science and Information Technology, Florida State University, Tallahassee, Florida 32306-4120

Jorge Viñals
Laboratory of Computational Genomics, Donald Danforth Plant Science Center, 975 North Warson Road, St. Louis, Missouri 63132

(Received 4 October 2001; published 2 April 2002)

We study numerically and analytically the coarsening of stripe phases in two spatial dimensions, and show that transient configurations do not achieve long ranged orientational order but rather evolve into glassy configurations with very slow dynamics. In the absence of thermal fluctuations, defects such as grain boundaries become pinned in an effective periodic potential that is induced by the underlying periodicity of the stripe pattern itself. Pinning arises without quenched disorder from the nonadiabatic coupling between the slowly varying envelope of the order parameter around a defect, and its fast variation over the stripe wavelength. The characteristic size of ordered domains asymptotes to a finite value $R_g \sim \lambda_0 \epsilon^{-1/2} \exp(|a|/\sqrt{\epsilon})$, where $\epsilon \ll 1$ is the dimensionless distance away from threshold, λ_0 the stripe wavelength, and a a constant of order unity. Random fluctuations allow defect motion to resume until a new characteristic scale is reached, function of the intensity of the fluctuations. We finally discuss the relationship between defect pinning and the coarsening laws obtained in the intermediate time regime.

DOI: 10.1103/PhysRevE.65.046119 PACS number(s): 64.60.−i, 64.70.Pf, 47.54.+r, 05.45.−a

I. INTRODUCTION

The motion of topological defects in two dimensional smectic phases is studied at a finite distance from threshold. We focus on the Swift-Hohenberg model of Rayleigh-Bénard convection and related amplitude equations to address the role that nonadiabatic effects play in domain coarsening of a modulated phase, defect pinning, and the appearance of glassy behavior.

Topological defects are often the longest lived modes of a nonequilibrium system, with their motion determining the longest relaxation times of the structure. Phenomenological models of defect motion that are based on a mesoscopic description have been known for some time [1,2]. Such a description, valid for distances much larger than the defect core, typically involves time-dependent Ginzburg-Landau equations or their generalizations. A few cases have been studied extensively, including domain coarsening in $O(N)$ models [3,4], in nematics [5–8], and in smectic phases as effectively encountered in models of Rayleigh-Bénard convection or lamellar phases of block copolymers [9–15]. In the case of modulated phases, the motion of a single defect has been widely studied within the well-known amplitude equation formalism. This method describes the spatiotemporal evolution of the envelope of a base periodic or modulated structure [16–20]. The amplitude equation description is valid only close to bifurcation points where the spatial scale of variation of the amplitudes is large or ''slow'' compared with the ''fast'' period of the base pattern and, in the present case, with the extent of the defect core as well.

Far enough from the bifurcation threshold of the modulated phase, the separation between slow and fast scales no longer holds, and corrections to the amplitude equations appear because of the coupling between both scales. These corrections are generically referred to as nonadiabatic effects. One manifestation of nonadiabaticity is that a defect that would be expected to move at constant velocity from an amplitude equation analysis may instead remain immobile or pinned [21–23]. We argue below that nonadiabatic effects and defect pinning have important consequences for domain coarsening of modulated phases in two dimensions, and are responsible for the formation of glassy configurations.

Our results complement recent research on glassy properties of stripe phases. It has been suggested that systems in which long ranged order is frustrated by repulsive interactions (the latter often leading to the formation of stripe phases or other patterns in equilibrium) may in fact exhibit the properties of structural glasses. An example are the glassy states, recently, observed in doped semiconductors in a stripe phase [24]. Coarse grained models with competing interactions of the type used here (and also used to study block copolymer melts in lamellar phases) have been reintroduced to describe the formation of glasses in supercooled liquids [25]. Additional equilibrium studies of the same models in three dimensions based on replica calculations [26] or Monte Carlo simulations [27] have been used to argue for the existence of an equilibrium glass transition. Structural glasses form spontaneously at low temperature without the presence of any quenched disorder, and their properties remain, in general, poorly understood. It is noteworthy that coarse grained models exhibiting glassy behavior in the absence of disorder are rare, whereas examples of discrete systems are known (e.g., Ising models with next-nearest-neigh-

*Present address: Instituto de Física, Universidad Nacional Autónoma de México, Apartado Postal 20-364, 01000 México D.F., Mexico.

bor interactions [28,29]). We present here a *two*-dimensional study that indicates a dynamical route to the formation of glassy configurations in stripe phases.

We first analyze the motion of a particular type of defect, namely, a grain boundary separating two domains of differently oriented stripes. Earlier asymptotic work near onset (i.e., in the limit $\epsilon \to 0$, where ϵ is the dimensionless distance away from threshold) is extended to the region of small but finite ϵ. In Sec. II, grain boundaries are shown to move in an effective periodic potential of wavelength $\lambda_0/2$ (where λ_0 is the periodicity of the stripe modulation) and of magnitude that increases very quickly with ϵ. Grain boundaries asymptotically pin as the driving force for grain boundary motion decreases. It is argued that for any finite ϵ an infinite size system will not achieve macroscopic long range order dynamically following a quench. Rather, the characteristic size of a domain will not exceed typical value R_g that is proportional to $\lambda_0\ \epsilon^{-1/2}\exp(|a|/\sqrt{\epsilon})$, where a is a constant of order unity.

In Sec. III, we incorporate the effect of random fluctuations and derive the corresponding amplitude equations valid for fluctuations of small amplitude. The asymptotic motion of a grain boundary can be recast as an escape problem in which the effective activation barrier is seen to be proportional to the grain boundary perimeter.

Our approach must be considered only qualitative in nature because of the scope of the description employed. Ginzburg-Landau equations, and more generally amplitude or order parameter equations (of which the Swift-Hohenberg model described below is but one example) are only asymptotic, large length scale approximations to the physical system they model in the immediate vicinity of a bifurcation point. Therefore, any short scale phenomena involved in the description of nonadiabatic corrections clearly falls beyond their range of validity, at least in a systematically quantifiable way. It is nevertheless not unreasonable to expect that nonadiabatic effects of the sort encountered in order parameter equations will also occur in the physical systems that they model. Furthermore, our results also provide insights into many existing numerical studies of these order parameter models, as described below.

In Sec. IV, we address the consequences of pinning on the domain coarsening that occurs in the intermediate time regime following the quench. This subject has been the focus of several numerical studies [10–15] and, more recently, of experimental studies in block copolymer thin films [30] and in electroconvection in nematics [31]. The results of Secs. II and III provide a possible interpretation of conflicting results in the literature. Previous studies of this problem [10–15] addressed the existence of self-similarity during domain coarsening and attempted to quantify the time dependence of the linear scale of the coarsening structure. The statistical self-similarity hypothesis asserts that after a possible transient, consecutive configurations of the coarsening structure are geometrically similar in a statistical sense. As a consequence, any linear scale of the structure (e.g., the average size of a domain or grain of like oriented stripes) is expected to grow as a power law of time $l(t) \sim t^{1/z}$, with z a characteristic exponent. Self-similarity is a well-known feature in systems that order in uniform phases of broken symmetry [32,33]. However, the determination of z has been problematic for stripe phases. Its value appears to depend on the quench depth (the value of ϵ), whether or not fluctuations are included in the governing equations, on the thermal history of the system, and on the particular linear scale analyzed.

Recent work in the limit $\epsilon \to 0$ showed that coarsening is self-similar and that $z=3$ [15]. The value $z=3$ in that limit can be justified by a dimensional analysis of the law of grain boundary motion. We focus here on the case of finite ϵ (in practice $\epsilon \geqslant 0.1$ for the Swift-Hohenberg model), and report a slowing down of phase ordering dynamics with increasing ϵ, in agreement with the literature. We attribute this behavior to partial pinning of defects that becomes increasingly important at long times as the driving force for coarsening decreases. At even longer times, coarsening stops altogether and the system reaches a glassy state as the linear scale of the structure reaches the critical value $R_g(\epsilon)$ computed in Sec. II. When random fluctuations are incorporated in the model, we show that, sufficiently close to onset, the value of z remains independent of the intensity of the fluctuations, thus verifying the universality implied in the self-similarity hypothesis in that region. At larger ϵ, we find that fluctuations accelerate ordering kinetics, also in agreement with the literature, and that, as expected, defect motion is allowed beyond the scale given by R_g. At even later times the system orders very slowly, possibly logarithmically in time.

II. NONADIABATIC CORRECTIONS AND GRAIN BOUNDARY PINNING

We consider the Swift-Hohenberg model of Rayleigh-Bénard convection [34] as a prototypical model of a modulated phase. The numerical results presented below have been obtained from a direct numerical solution of the model. The analytic results, on the other hand, follow from the corresponding amplitude equation, and hence are expected to be of somewhat wider generality. The model equation studied here is

$$\frac{\partial \psi}{\partial t} = \epsilon \psi - \frac{1}{k_0^4}(k_0^2 + \nabla^2)^2 \psi - \psi^3, \tag{1}$$

where ψ is a dimensionless order parameter related to the vertical fluid velocity at the midplane of a Rayleigh-Bénard convection cell, ϵ is the reduced Rayleigh number $(R - R_c)/R_c \ll 1$ (R_c is the critical Rayleigh number for instability), and $k_0 = 2\pi/\lambda_0$ is the roll wave number (in Appendix A we outline the connection between this model and other coarse-grained models with long range repulsive interactions [35]).

For $0 < \epsilon \ll 1$, the leading order approximation to the stationary solution of Eq. (1) is a sinusoidal function of wave number k_0. We focus in this section on a configuration that contains an isolated grain boundary separating two such stationary solutions with mutually perpendicular wave vectors (Fig. 1). The reason for studying this perpendicular orientation is the expectation that a 90° grain boundary is that of lowest energy, and hence the prevalent boundary angle in an

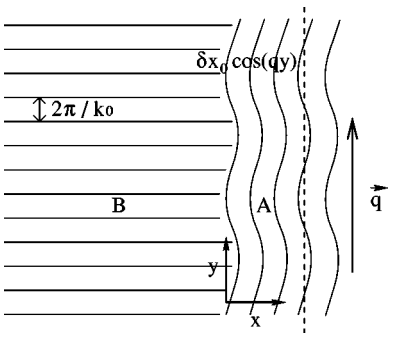

FIG. 1. Schematic grain boundary configuration separating two domains of stripes A and B of the same periodicity ($|\vec{k}_0|=|\vec{k}_0'|=k_0$). The stripes of domain A are weakly curved by a transverse modulation of wave number $q \ll k_0$. δx_0 represents the magnitude of the phase modulation.

extended system that evolves spontaneously from an initially disordered configuration [see, for example, Figs. 3(a), 3(b)]. It is known that a planar grain boundary separating two regions of uniform k_0 is stationary [19,20]. However, we found in Ref. [36] that a slightly perturbed boundary undergoes a net translation with a speed that is a function of the curvature of the rolls ahead of it. We address in this section the extension of the asymptotic results given in that reference to small but finite ϵ, and show how corrections obtained lead to boundary pinning.

Near threshold, a 90° grain boundary configuration is an approximate solution of Eq. (1) of the form

$$\psi(x,y,t)=\tfrac{1}{2}[A(X_A,Y_A,T)e^{ik_0x}+B(X_B,Y_B,T)e^{ik_0y}+\text{c.c.}], \tag{2}$$

where slow variables are denoted by capital letters and are defined as [19,20]

$$X_A=\epsilon^{1/2}x,\quad Y_A=\epsilon^{1/4}y;\quad X_B=\epsilon^{1/4}x,\quad Y_B=\epsilon^{1/2}y;\quad T=\epsilon t. \tag{3}$$

(The coordinate x is directed along the normal to the reference planar boundary.)

We recall first some known results for a planar and stationary grain boundary in the limit $\epsilon\to 0$, a case that was extensively studied in Refs. [19,20]. The stationary amplitudes $\{A_0,B_0\}$ are a function only of x. A_0, the amplitude of the rolls parallel to the interface, vanishes as $\exp(x\sqrt{\epsilon}/\lambda_0)$ when $x\to-\infty$, and saturates to $(4\epsilon/3)^{1/2}\tanh(x\sqrt{\epsilon}/\lambda_0)$ when $x\to+\infty$. The behavior of the amplitude of the rolls perpendicular to the interface is slightly different: $B_0(x)-(4\epsilon/3)^{1/2}\propto\exp(x\sqrt{\epsilon}/\xi_0)$ when $x\to-\infty$ and there exists a location x^* such that $B_0(x>x^*)\simeq 0$ to a good approximation. Hence, the grain boundary region has a thickness proportional to $\lambda_0/\sqrt{\epsilon}$. It is important to note that at small ϵ the location of the grain boundary decouples from the phase of the stripes of domain A. Thus, the configuration obtained is invariant under any translation of the grain boundary by a distance x_0 (the phase of the stripes remaining unchanged).

We next derive two coupled equations for the amplitudes A and B that take into account the possible coupling between these amplitudes and the phases of the stripes. This coupling becomes significant at a finite value of ϵ, and hence when there is a large but finite separation between the scales $\{X_{A,B},Y_{A,B}\}$ and $\{x,y\}$. We follow an approach similar to that used in Ref. [23] to study the motion of a planar front between a hexagonal and a uniform phase, or between a hexagonal and a stripe phase. The first step is a multiscale analysis, and is standard [16]. Equation (1) is expanded in power series of ϵ, as well as the solution $\psi=\epsilon^{1/2}\psi_{1/2}+\epsilon\psi_1+\epsilon^{3/2}\psi_{3/2}+\cdots$. The leading order solution $\epsilon^{1/2}\psi_{1/2}$ is given by Eq. (2). At order $\epsilon^{3/2}$, the solvability conditions for the existence of a nontrivial solution for $\psi_{3/2}$ yield the relations that A and B must satisfy,

$$\int_x^{x+\lambda_0}\lambda_0^{-1}dx'\int_y^{y+\lambda_0}\lambda_0^{-1}dy'[\mathcal{L}(\psi_{1/2})-\psi_{1/2}^3]e^{-ik_0x'}=0, \tag{4}$$

$$\int_x^{x+\lambda_0}\lambda_0^{-1}dx'\int_y^{y+\lambda_0}\lambda_0^{-1}dy'[\mathcal{L}(\psi_{1/2})-\psi_{1/2}^3]e^{-ik_0y'}=0, \tag{5}$$

with the linear operator $\mathcal{L}=1-\partial_T-k_0^{-4}(\partial_{X_B}^2+\partial_{Y_A}^2+2\partial_y\partial_{Y_B}+2\partial_x\partial_{X_A})^2$. In the limit $\epsilon\to 0$ the functions A and B remain constant over one spatial period λ_0, and therefore, the only nonvanishing contribution to the integrals come from the terms proportional to $e^{ik_0x'}$ (resp. $e^{ik_0y'}$) within brackets in Eq. (4) [resp. Eq. (5)]. This standard set of coupled Ginzburg-Landau equations follows [16,19]. It is known, however, that additional nonperturbative contributions arising from the term $\psi_{1/2}^3$ appear in Eqs. (4) and (5). We focus next on these contribution and their effect on the relaxation of a slightly perturbed grain boundary.

Integrals of the type $\int_x^{x+\lambda_0}dx'\,e^{imk_0x'}A^nB^p$ in Eqs. (4) and (5) (where m, n, and p are integers) will not integrate to zero if the thickness of the grain boundary profiles along the x direction is finite. (Contributions from the direction transverse to the grain boundary, $\int_y^{y+\lambda_0}dy'\,e^{imk_0y'}A^nB^p$, will be neglected. They are typically of the order of $B^2\partial_y^2A$ and, hence, always smaller than the leading analytical terms of the amplitude equations.) Terms proportional to $e^{imk_0x'}$ will contribute to Eq. (4), and terms proportional to $\exp[imk_0x'+ik_0y']$ to Eq. (5). If we only retain the lowest order term $\epsilon^{1/2}\psi_{1/2}$ as given by Eq. (2), we find that only A^3 ($m=3$) contributes to Eq. (4), while $3A^2B$ ($m=2$), as well as $3\bar{A}^2B$ ($m=-2$, with $\bar{A}$ the complex conjugate of A), to Eq. (5). Reintroducing the original unscaled variables, the generalized amplitude equations read

$$\frac{\partial A}{\partial t}=-\frac{\delta F_{gb}}{\delta\bar{A}}-\frac{1}{4\lambda_0^2}\int_x^{x+\lambda_0}dx'\times\int_y^{y+\lambda_0}dy'\,A^3(x',y',t)e^{i2k_0x'}, \tag{6}$$

$$\frac{\partial B}{\partial t} = -\frac{\delta F_{gb}}{\delta \overline{B}} - \frac{3}{4\lambda_0^2}\int_x^{x+\lambda_0} dx' \int_y^{y+\lambda_0} dy' \times [A^2 B e^{i2k_0 x'} + \overline{A}^2 B e^{-i2k_0 x'}], \tag{7}$$

where $F_{gb} = \int d\vec{r}\mathcal{F}_{gb}$ is the standard Lyapunov functional corresponding to the 90° grain boundary. Its variational derivatives satisfy [19,20]

$$-\delta F_{gb}/\delta \overline{A} = \epsilon A + \frac{4}{k_0^2}\left(\partial_x - \frac{i}{2k_0}\partial_y^2\right)^2 A - \frac{3}{4}|A|^2 A - \frac{3}{2}|B|^2 A, \tag{8}$$

$$-\delta F_{gb}/\delta \overline{B} = \epsilon B + \frac{4}{k_0^2}\left(\partial_y - \frac{i}{2k_0}\partial_x^2\right)^2 B - \frac{3}{4}|B|^2 B - \frac{3}{2}|A|^2 B. \tag{9}$$

The last terms in the right-hand sides of Eqs. (6) and (7) depend on both fast and slow spatial scales, and they embody the so-called nonadiabatic coupling between the two. Analyzing the effects of these two terms on the relaxation of a perturbed grain boundary is the subject of the remainder of this section.

We now introduce a small perturbation to the planar boundary as shown schematically in Fig. 1. The phase of the stripes of domain A is distorted by a uniform perturbation of wave number $q \ll k_0$ (and of amplitude $\delta x_0 \ll \lambda_0$) in the direction transverse to the stripes. As shown in Ref. [36], approximate solutions to Eqs. (6) and (7) are given by

$$A = A_0[x - x_{gb}(t)]\exp[ik_0 \delta x_0 \cos(qy)], \tag{10}$$

$$B = B_0[x - x_{gb}(t)], \tag{11}$$

where $x_{gb}(t)$ represents the time-dependent position of the grain boundary (averaged over y). As already discussed in that reference, perturbations to the phase of B are of higher order in ϵ. In order to derive a law of motion for x_{gb} it is simpler to neglect the linear relaxation of the perturbed rolls, and hence, assume that δx_0 is constant. The amplitude δx_0 relaxes exponentially with time but the relaxation time of the perturbation is proportional to q^{-4} and usually much longer than the characteristic time associated with grain boundary motion, $\lambda_0/\dot{x}_{gb}$. Furthermore, as was shown in Ref. [36], explicitly considering stripe relaxation does not change the law of motion for x_{gb} in any quantitative way.

Multiply Eq. (6) [resp. Eq. (7)] by $\partial_t \overline{A}$ (respectively $\partial_t \overline{B}$), add the results and integrate the real part over the system area. By using Eqs. (10) and (11) and integrating by parts the nonadiabatic terms, we obtain the following law of motion for the grain boundary,

$$\dot{x}_{gb} = \frac{\epsilon}{3k_0^2 D(\epsilon)}\kappa^2 - \frac{p(\epsilon)}{D(\epsilon)}\cos(2k_0 x_{gb} + \phi), \tag{12}$$

where $\kappa = \delta x_0 q^2$ is proportional to the mean curvature of the stripes of domain A, ϕ is a constant phase, and

$$D(\epsilon) = \int_{-\infty}^{\infty} dx[(\partial_x A_0)^2 + (\partial_x B_0)^2], \tag{13}$$

$$p(\epsilon) = \max_\theta \left\{ \frac{3}{4}\int_{-\infty}^{\infty} dx\, A_0^3(x)\partial_x A_0(x)\cos(2k_0 x + \theta) + \frac{3}{2}\int_{-\infty}^{\infty} dx[2A_0 B_0^2 \partial_x A_0 + A_0^2 B_0 \partial_x B_0] \times \cos(2k_0 x + \theta) \right\}. \tag{14}$$

Equation (12) without the oscillatory term was derived in Ref. [36] in the limit $\epsilon \to 0$. The coefficient $D(\epsilon)$, with dimensions of an inverse length, represents a friction term that depends on the static grain boundary profile $\{A_0, B_0\}$, while the term $\epsilon\kappa^2$ in the numerator is proportional to $\int_0^L dy[\mathcal{F}_{gb}(x=\infty,y) - \mathcal{F}_{gb}(x=-\infty,y)]/L$, where $\mathcal{F}_{gb}$ is the free energy density implicitly defined by Eqs. (8) and (9). The numerator can be understood as the leading contribution (in ϵ and κ) from an external force acting on the grain boundary. This force results from the difference in the free energy density $\mathcal{F}_{gb}$ between curved stripes on one side, and straight stripes on the other side of the boundary. Note the unusual dependence of $\dot{x}_{gb}$ on a even power of the curvature thus indicating that the motion of the grain boundary is such that curved parallel rolls of higher energy are always replaced by straight perpendicular rolls.

The last term in the right-hand side of Eq. (12) is the dominant contribution arising from the nonadiabatic terms of Eqs. (6) and (7). The *dimensionless* quantity $p(\epsilon)$ plays the role of the amplitude of a periodic potential of period $\lambda_0/2$ within which the grain boundary moves. The major contribution to $p(\epsilon)$ comes from the integral that contains the term $\partial_x B_0$ in Eq. (14) since the profile $B_0(x)$ has a steeper variation than $A_0(x)$ [19]. Given that both amplitudes A_0 and B_0 are approximately of the form $\sqrt{\epsilon} f(\sqrt{\epsilon}x/\lambda_0)$, it is easy to show from Eq. (14) that

$$p(\epsilon) \sim \epsilon^2 e^{-|\alpha|/\sqrt{\epsilon}}, \tag{15}$$

where $|\alpha|$ is a constant of order unity, corresponding to the pole of the envelopes closest to the real axis in the complex plane. Hence, p behaves nonanalytically at small ϵ, and increases extremely quickly with ϵ. Qualitatively similar results were reported in Refs. [22,23] for one dimensional fronts between conductive and convective states, or between different convective states.

Equation (12) shows that for any finite $\epsilon > 0$ a planar grain boundary ($\kappa = 0$) can have only two stationary positions per period of the stripe pattern λ_0. This effect had been observed numerically and reported in Ref. [36], with similar findings also given in Ref. [20]. Equation (12) also implies that there exists a critical curvature κ_g below which the grain boundary will remain immobile. This critical curvature is given by,

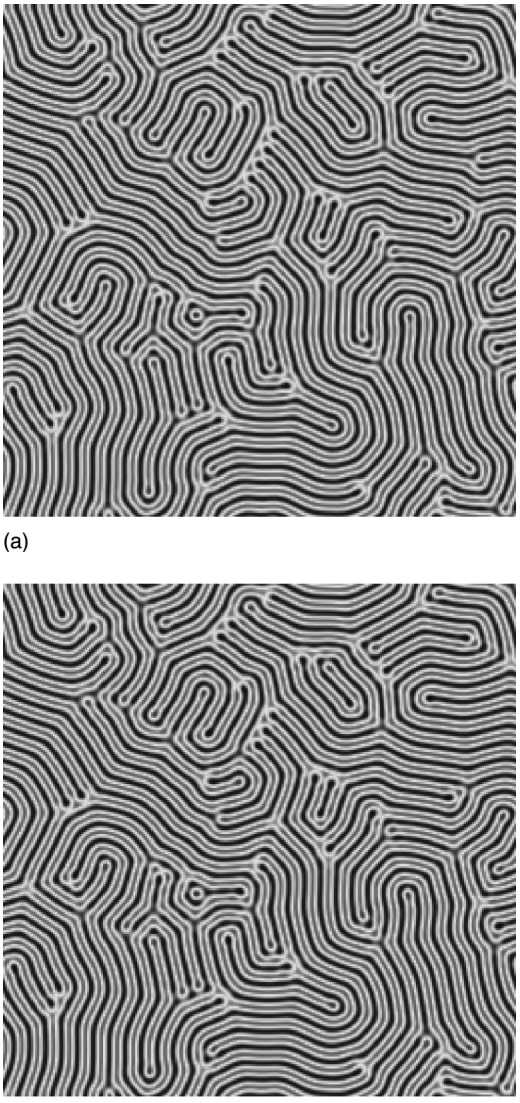

FIG. 2. Glassy configurations obtained by numerical solution of the Swift-Hohenberg model with random initial conditions. Dimensionless times shown are (a) $t=10\,000$ and (b) $t=20\,000$. Here $\epsilon=0.5$ and the system has 256^2 grid nodes.

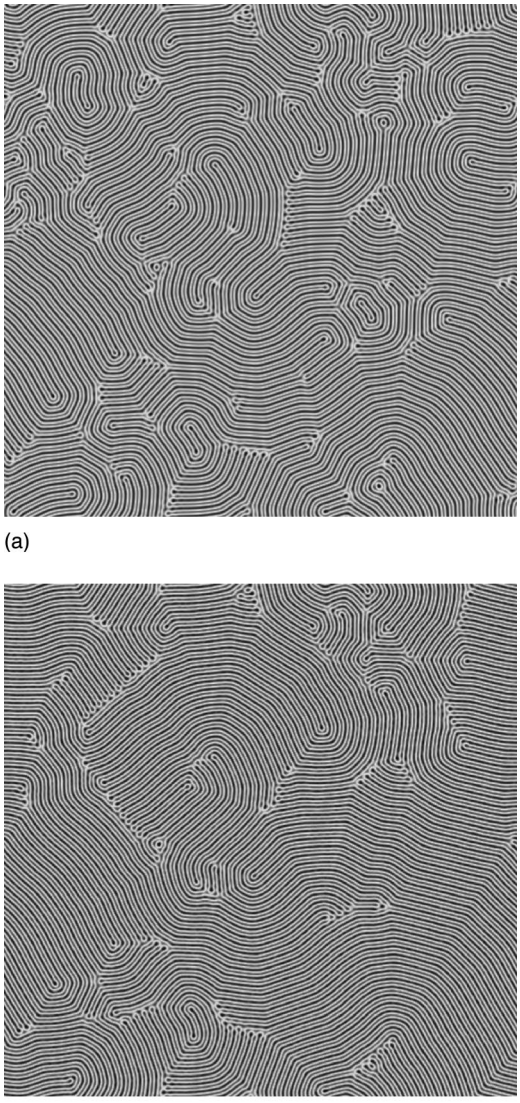

FIG. 3. (a) Near stationary configuration obtained after a quench at $\epsilon=0.4$ and in the absence of fluctuations $F=0$ (the time shown is $t=2.3\times10^5$, and the system size includes 512^2 nodes). (b) New structure obtained after taking the configuration shown in (a) as an initial condition and further integrating the model equations with $F=0.00\,318$ for a period of 10^5 time units. At this time, any boundary motion is very slow.

$$\kappa_g=\frac{1}{R_g}=k_0\left(\frac{3p(\epsilon)}{\epsilon}\right)^{1/2}, \tag{16}$$

where R_g is the associated radius of curvature that diverges nonanalytically near onset [see Fig. 5(a)]

$$R_g\sim\lambda_0\epsilon^{-1/2}\exp\left(\frac{|\alpha|}{2\sqrt{\epsilon}}\right). \tag{17}$$

These results have been verified by direct numerical solution of the Swift-Hohenberg model with reasonably small values of ϵ. The numerical algorithm used has been described in Refs. [15,36]. Briefly, Eq. (1) is discretized on a square grid of mesh size $\Delta x=1$ with 512^2 nodes (256^2 for $\epsilon=0.5$), and the wavelength is set to $\lambda_0=8\Delta x$. A semi-implicit spectral method is used to iterate in time. The initial condition for ψ is a white and Gaussian random field with zero average and variance $\langle\psi^2\rangle=\epsilon$. Typical long time configurations that are stationary for all practical purposes are shown in Figs. 2(a) and 2(b). These figures show the field ψ in gray scale. Many topological defects including dislocations, $+1/2$ disclinations, and several 90° grain boundaries can be identified. Figure 2 corresponds to $\epsilon=0.5$ and two different times $t=10^4$ and $t=2\times10^4$, showing that the order parameter does not change beyond $t=10^4$. Figure 3(a) corresponds to $\epsilon=0.4$, and the configuration shown remains practically constant beyond $t=2.3\times10^5$.

To further quantify these observations we have computed the probability distribution function of stripe curvatures

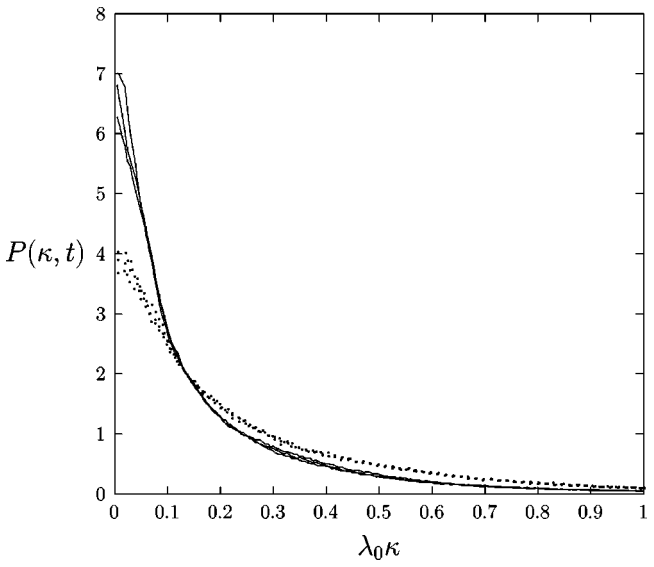

FIG. 4. Probability distribution function of stripe curvatures, $P(\kappa,t)$, after a quench at $\epsilon=0.5$ (dotted lines) and $\epsilon=0.4$ (solid lines), averaged over 10 and 6 independent runs, respectively. For $\epsilon=0.5$ the figure shows the curves obtained at times $t=10^4$, 5×10^4, and 10^5, and for $\epsilon=0.4$ at times $t=6\times10^4$, 1.2×10^5, and 2.3×10^5.

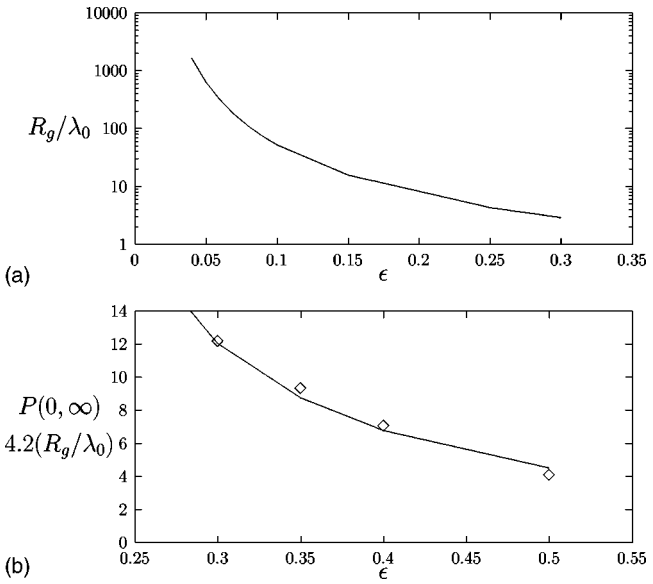

FIG. 5. Characteristic asymptotic grain size following a quench as a function of ϵ. (a) Estimate given by Eq. (16). (b) Numerical value of $P(\kappa=0,t=\infty)$ (symbols) compared also with Eq. (16) multiplied by one fitted scale factor (solid line).

$P(\kappa,t)$. The stripe curvature is defined as $\kappa=|\vec{\nabla}\cdot\hat{n}|$, where $\hat{n}$ is the unit normal to the lines of constant ψ. The curvature κ is a slowly varying quantity away from defect cores, and only these regions are used to compute $P(\kappa,t)$ by the filtering method described in Ref. [15]. Figure 4 shows our results for $\epsilon=0.4$ and $\epsilon=0.5$. In both cases the distribution converges at long times towards a limiting curve of finite width, thus indicating that asymptotic configurations contain many curved stripes and are disordered at large or ''glassy'' scales. This behavior is to be contrasted with that of a coarsening system in which $P(\kappa,t\to\infty)$ would approach a δ function at $\kappa=0$. We take $P(\kappa=0,t\to\infty)$ as a measure of the linear scale of the structure or typical domain size and compare its value with the pinning radius R_g given in Eq. (16). Figure 5(b) shows the numerical results together with R_g multiplied by a (fitted) scale factor approximately equal to 4. The pinning radius R_g increases extremely quickly with decreasing ϵ, in agreement with the numerical calculations for the range of ϵ, we can study (computational constraints on system sizes have prevented us from investigating the region $\epsilon<0.30$). We have checked that the glassy configurations at long times do not result from numerical pinning; the results are not modified when the grid spacing is halved to $\Delta x=\lambda_0/16$.

Although other types of defects (e.g., dislocations and $+1/2$ disclinations) may also become pinned, and thus contribute to the overall stability of glassy configurations, the predominance of grain boundaries over other defects seems to be a generic feature of the Swift-Hohenberg model [see Figs. 2(a), 2(b), 3(a), 3(b), and Ref. [15]]. Furthermore it is likely that a similar dependence between the speed of the defect and ϵ will hold for the motion of other topological defects (except for dislocation climb). Hence, we argue that a defected configuration of stripes does not macroscopically order following a quench to a finite value of ϵ. Asymptotic long time configurations appear to exhibit a labyrinthic and partially disordered structure with many immobile defects that do not anneal away. These disordered configurations resemble those of a structural glass at zero temperature that lack long range order (translational or orientational). They become spontaneously trapped in metastable configurations that are very different from the configuration of lowest free energy (all stripes parallel to each other, or a ''crystalline'' state).

Not all grain boundaries in a glassy configuration are 90° boundaries. However, we expect that grain boundaries with a different orientation would be pinned less efficiently [i.e., would have a higher value of $|\alpha|$ in Eq. (15)]. The reason is that their stationary planar profile is smoother than that of a 90° grain boundary, and therefore, nonadiabatic effects are expected to be weaker.

We finally mention that if both ϵ and $\kappa\lambda_0$ are not small compared to one, both adiabatic and nonadiabatic terms will contain higher-order analytic corrections that we have not calculated.

III. MOTION AT FINITE TEMPERATURE

Given the results of Sec. II, it is natural to study the effect of random fluctuations added to Eq. (1). Small amplitude fluctuations will allow activated motion of grain boundaries, and in general, unpinning. We consider in this section the stochastic Swift-Hohenberg model

$$\frac{\partial\psi}{\partial t}=\epsilon\psi-\frac{1}{k_0^4}(k_0^2+\nabla^2)^2\psi-\psi^3+\eta(\vec{r},t), \qquad (18)$$

where η is a Gaussian and white random noise of zero mean and variance

$$\langle \eta(\vec{r},t)\,\eta(\vec{r}',t')\rangle = 2F\,\delta(\vec{r}-\vec{r}')\,\delta(t-t'). \tag{19}$$

The noise intensity F is proportional to the (dimensionless) temperature according to the fluctuation-dissipation theorem. In what follows, F and ϵ are considered as independent parameters, although they might be related in some particular physical systems. The stochastic Swift-Hohenberg model has been used to study hydrodynamic fluctuations near onset of Rayleigh-Bénard convection [37], and thermal fluctuations of molecular origin in lamellar phases of diblock copolymers [38].

The stationary states of Eq. (18) in two spatial dimensions have been studied in Refs. [11,39]. Above a critical noise intensity F_c (that depends on ϵ), the system is disordered (lacks both translational and orientational long ranged order). Below F_c a stripe phase with long ranged orientational order but no translational order was found. Only at $F=0$ the system was seen to exhibit both translational and orientational long ranged order. In what follows we focus on defect dynamics in the range $0<F\ll F_c$, so that the local stripe pattern is not very distorted.

We first derive the stochastic amplitude equations for a 90° grain boundary. Following Graham [40], we approximate the effect of the noise on the amplitudes by projecting it along the two slow modes of the deterministic equation and neglecting any contribution arising from couplings and resonances between noise and fast variables [41,42]. We start by writing the random function as,

$$\eta(\vec{x},t)=\tfrac{1}{2}[e^{ik_0x}\tilde{\eta}_A(X_A,Y_A,T)+e^{ik_0y}\tilde{\eta}_B(X_B,Y_B,T)+\text{c.c.}], \tag{20}$$

where the slow variables $X(Y)_{A,B}$ are given by Eq. (3), and $\tilde{\eta}_A$ and $\tilde{\eta}_B$ are two independent complex random processes that satisfy the relations,

$$\langle\tilde{\eta}_A\rangle=\langle\tilde{\eta}_B\rangle=0,\ \langle\tilde{\eta}_A^2\rangle=\langle\tilde{\eta}_A\tilde{\eta}_B\rangle=\langle\tilde{\eta}_A\tilde{\eta}_B^*\rangle=0,$$

$$\langle\tilde{\eta}_A\tilde{\eta}_A^*\rangle=\langle\tilde{\eta}_B\tilde{\eta}_B^*\rangle=2F\,\delta(\vec{x}-\vec{x}')\,\delta(t-t').$$

It is implicit in the decomposition that F is small enough so that well-defined stripes exist locally. On the other hand, F has to be large enough so that $\tilde{\eta}_A$ and $\tilde{\eta}_B$ are not negligible in the solvability conditions at order $\epsilon^{3/2}$ [43]. Given both assumptions, Eqs. (6) and (7) straightforwardly generalize to

$$\frac{\partial A}{\partial t}=-\frac{\delta F_{gb}}{\delta\overline{A}}-\frac{1}{4\lambda_0^2}\int_x^{x+\lambda_0}dx'\times\int_y^{y+\lambda_0}dy'A^3(x',y',t)e^{i2k_0x'}+\tilde{\eta}_A, \tag{21}$$

$$\frac{\partial B}{\partial t}=-\frac{\delta F_{gb}}{\delta\overline{B}}-\frac{3}{4\lambda_0^2}\int_x^{x+\lambda_0}dx'\times\int_y^{y+\lambda_0}dy'[A^2Be^{i2k_0x'}+\overline{A}^2Be^{-i2k_0x'}]+\tilde{\eta}_B. \tag{22}$$

We can now estimate the escape rate of a grain boundary over the potential barrier of Eq. (12). In order to do so, we need to estimate the projection of the noise intensity in Eqs. (21) and (22) on the coordinate $x_{gb}(t)$ implicitly defined by Eqs. (10) and (11). A rough estimate that is sufficient for our purposes can be obtained by using Eqs. (10) and (11) as the trial solution of Eqs. (21) and (22). Focusing on x_{gb} alone ignores possible boundary broadening because of fluctuations, or roughening. Both phenomena will be important for grain boundary motion above the pinning point, but their contribution is probably less important in the immediate vicinity of the pinning transition. By substituting Eqs. (10) and (11) into Eqs. (21) and (22), we find

$$\dot{x}_{gb}=\frac{\epsilon}{3k_0^2D(\epsilon)}\kappa^2-\frac{p(\epsilon)}{D(\epsilon)}\cos(2k_0x_{gb}+\phi)+\tilde{\eta}, \tag{23}$$

with $\tilde{\eta}$ a (real) random white Gaussian noise satisfying,

$$\langle\tilde{\eta}\rangle=0,\quad\langle\tilde{\eta}(t)\tilde{\eta}(t')\rangle=2F'\,\delta(t-t'),$$
$$F'=F/[2D(\epsilon)R_{gb}], \tag{24}$$

where R_{gb} is the grain boundary perimeter. As expected, the intensity of the fluctuations on the global coordinate x_{gb} is proportional to $1/R_{gb}$. Equation (23) is a straightforward generalization of Eq. (12), and is formally analogous to the equation that describes the one-dimensional motion of a Brownian particle in a periodic potential of amplitude $2p(\epsilon)/[2D(\epsilon)k_0]$.

Equations (23) and (24) can be recast as

$$\dot{x}_{gb}=\left(\frac{k_0F_0}{2D}\right)R_g\kappa^2-\left(\frac{k_0F_0}{2D}\right)\frac{1}{R_g}\cos(2k_0x_{gb}+\phi)+\frac{1}{\sqrt{2D}}\left(\frac{F}{R_{gb}}\right)^{1/2}\xi. \tag{25}$$

The random term ξ is such that $\langle\xi\rangle=0$ and $\langle\xi(t)\xi(t')\rangle=2\,\delta(t-t')$. We have also used Eq. (16) to eliminate $p(\epsilon)$ from Eq. (23), and we have defined

$$F_0=\frac{2\epsilon}{3k_0^3R_g}. \tag{26}$$

Consider the situation where grain boundaries are pinned at $F=0$. Since $\kappa<\kappa_g$, the first term of the right-hand side of Eq. (25) is not dominant and the potential barrier that a pinned defect of size R_{gb} has to overcome is of the order of F_0/R_g. The stochastic problem is now an escape problem

over this potential barrier given the intensity of the noise term in Eq. (25). The Kramers rate of escape is given by

$$r \sim \exp\left(-\frac{F_0}{F}\frac{R_{gb}}{R_g}\right). \tag{27}$$

Therefore, a noise intensity

$$F = R_{gb}\frac{F_0}{R_g} \sim R_{gb}k_0^{-1}\epsilon^2 e^{-|\alpha|/\sqrt{\epsilon}} \tag{28}$$

is required to unpin a grain boundary of length R_{gb}.

IV. SLOW COARSENING DYNAMICS: DEPENDENCE ON TEMPERATURE AND QUENCH DEPTH

We use here the results of Secs. II and III to provide a possible interpretation of conflicting results concerning domain coarsening of stripe phases. We recently studied this issue by numerically solving the *noiseless* Swift-Hohenberg equation [Eq. (1)] *in the limit* $\epsilon \to 0$ [15]. Our numerical results suggested that the characteristic scale of the structure (or the typical size of ordered domains) increases as $t^{1/z}$, with $z=3$. That value of the exponent was interpreted to follow from the dominant motion of grain boundaries through a background of curved stripes. In disordered configurations, the curvature of stripes is set by a distribution of largely immobile $+1/2$ disclinations. According to Eq. (12), the motion of grain boundaries is driven by stripe curvature, and acts to reduce the overall curvature by replacing regions of curved stripes by straight ones of a different orientation. It also reduces the disclination density whenever their core region is swept by a moving grain boundary. In the limit $\epsilon \ll 1$ we computed several measures of the linear scale, including moments of $P(\kappa,t)$, moments of the structure factor of the order parameter, and the average distance between defects. They were all found to become proportional to each other, and to grow as a power law of time with an exponent 1/3.

Grain boundary motion as described in Sec. II was used to provide an interpretation for the value $z=3$. Since $+1/2$ disclinations generate roughly axisymmetric patterns of stripes around them, the characteristic stripe curvature in any given configuration is proportional to the inverse characteristic distance between disclinations. Under the self-similarity hypothesis, the distance between disclinations is proportional to the grain size $l(t)$, hence $\kappa \sim 1/l(t)$. If grain boundaries are the class of defect, the motion of which controls asymptotic coarsening, then the coarsening exponent can be inferred by dimensional analysis of Eq. (12). In the limit $\epsilon \to 0$, the oscillatory term in the right-hand side of Eq. (12) can be neglected and we simply have $dl/dt \propto l^{-2}$ or $l(t) \sim t^{1/3}$, in agreement with the numerical solution of Eq. (1).

Equation (12) shows that this result changes qualitatively further from onset. As ϵ increases the pinning potential energy barrier $p(\epsilon)$ increases extremely fast, and important corrections to scaling are to be expected. For finite ϵ and short times many defects are present, therefore, the characteristic curvature of the stripes is very large, and the first term in the right-hand side of Eq. (12) dominates. As coarsening proceeds, the characteristic curvature decreases until it reaches the critical value κ_g given by Eq. (16). At that point the typical velocity of a grain boundary vanishes, although the system is still disordered. Therefore, one would expect that coarsening would stop when $l(t)$ is of the order of R_g. This is precisely the result shown in Fig. 5(b) with only one adjustable parameter [a scale factor relating R_g given by Eq. (16) to $l(t)$ determined numerically from the distribution of stripe curvatures].

When random fluctuations are considered [$F>0$ in Eqs. (18) and (19)], some of the grain boundaries in a frozen configuration are expected to resume motion. We argue that the structure will continue coarsening until the average domain size reaches a new characteristic size $l_F > R_g$ that can be estimated as follows. We write a general phenomenological evolution equation for the domain size $l(t)$ directly from Eq. (25):

$$\frac{dl}{dt} = \left(\frac{k_0F_0}{2D}\right)\frac{R_g}{l^2} - \left(\frac{k_0F_0}{2D}\right)\frac{1}{R_g}\cos(2k_0l+\phi) + \frac{1}{\sqrt{2D}}\left(\frac{F}{l}\right)^{1/2}\xi, \tag{29}$$

where we have assumed that, prior to pinning, the various length scales remain approximately proportional to each other. Recall from Eq. (27) that $F=F_0$ is required to unpin a configuration obtained in the absence of noise, for which $R_{gb} \sim l(t) \sim R_g$. According to Eq. (29), coarsening proceeds if $F>F_0$ until a new characteristic pinning size is reached given by $F_0 l_F/(FR_g)=1$ or

$$l_F = R_g\frac{F}{F_0} \sim k_0 F\frac{e^{|\alpha|/\sqrt{\epsilon}}}{\epsilon^2}. \tag{30}$$

After reaching the scale l_F, domains are expected to coarsen very slowly by thermal activation. When a grain boundary overcomes one pinning barrier, the linear extent of the corresponding domain typically increases by an amount of order $\lambda_0/2$. Hence, $dl/dt \sim \lambda_0 r$, where r is given by Eq. (27) with R_{gb} replaced by l. Hence, domains are expected to grow logarithmically in time according to

$$l(t) \sim F\ln(t/F) \quad \text{for} \quad l \gg l_F. \tag{31}$$

A numerical solution of Eq. (18) yields results qualitatively consistent with those presented above. Figure 3(a) shows a configuration of the order parameter field ψ obtained for $F=0$ and $\epsilon=0.4$ starting from random initial conditions. The configuration shown corresponds to very late times $t=2.3\times10^5$ at which point all defects are practically immobile, and domain growth has stopped. We then set $F=0.003\,18$, and the integration is continued. The order parameter configuration $t=10^5$ time units later is shown in Fig. 3(b). The average domain size has increased substantially. Many grain boundaries have a 90° orientation [such as in Fig. 3(a)], and roughening is limited or nonexistent. We have determined the average domain size l from the probability distribution function of the quantity $\zeta = \psi^2 + (\vec{\nabla}\psi)^2/k_0^2$. Figure 6 shows the probability distribution function correspond-

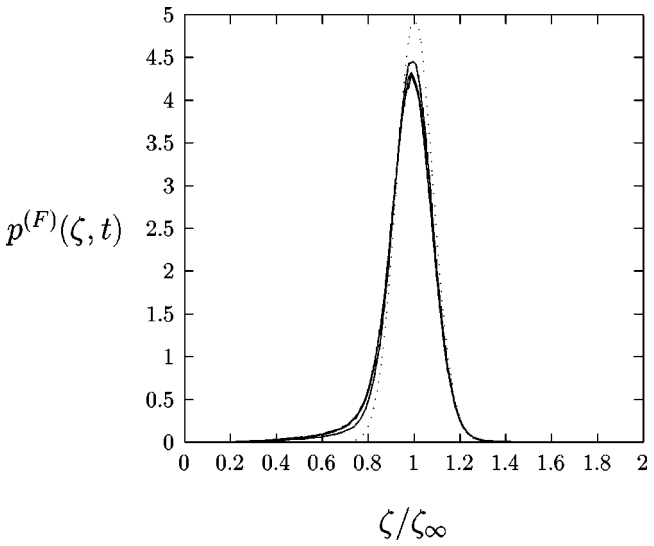

FIG. 6. Probability distribution function of ζ defined by Eq. (B1) with ψ the solution of Eq. (18) for $F=0.00\,636$ and $\epsilon=0.4$. The dotted line corresponds to a single plane wave with superimposed fluctuations, while the solid line correspond to disordered configurations obtained from random initial conditions (at times $t=5\times10^3$, 10^4, and 10^5, respectively).

ing to a perfectly ordered configuration, as well as to partially disordered configurations. The inverse linear scale $1/l$, proportional to the defect density ρ_d, is extracted from the difference between these curves, as detailed in Appendix B. As shown in Fig. 7 domain growth is very slow, possibly logarithmic, although a precise check of this behavior is problematic.

Figure 8 displays the evolution of the defect density $\rho_d(t)$ as a function of time, starting from random initial configurations. For reference we also show the case $F=0$. Increasing the value of ϵ leads to smaller effective exponents, whereas increasing F has the opposite effect. For sufficiently small ϵ, we find $z=3$ independent of the value of F. The two bottom curves correspond to systems that are close enough to onset, and hence either R_g or l_F is very large compared with the linear size of the system. We show our results for $\epsilon=0.04$ (averaged over 40 independent runs) and for $\epsilon=0.15$ (averaged over 15 independent runs). The solid line closest to these two curves has a slope of $-1/3$. The downward deviation from linearity at long times at $\epsilon=0.04$ is a typical manifestation of finite size effects (this long time behavior and its dependence on the system size was studied in detail in Ref. [15]).

With increasing ϵ and/or decreasing F, pinning becomes more pronounced as evidenced the lower effective slopes of the three upper curves in Fig. 8 (the results are averages over six independent runs, each curve corresponding to the same value $\epsilon=0.4$). The top curve corresponds to a system without fluctuations for which ρ_d was computed with the method described in Ref. [15]. The density starts decaying roughly as an inverse power law, with an effective exponent much smaller than $-1/3$ (the top solid line has a slope of $-1/5$), and after a crossover saturates at long times indicating pinning. When small amplitude noise is added (curve below denoted by diamonds), the initial behavior is similar to that of $F=0$, and the decay rate also slows down considerably at long times [where we would predict logarithmic growth, i.e., $\rho_d\sim1/\ln(t)$]. The curve below, denoted by plus signs, corresponds to a noise intensity three times larger than the previous case. Its initial decay is slightly faster (it can be fitted with an effective exponent $1/z_{eff}\simeq-0.23$ as shown with the solid line in the figure), and the upwards deviations at long times are less pronounced. This behavior is in qualitative agreement with the the expectation that defects overcome pinning barriers more readily at higher noise intensities and pinning is postponed to longer times when $l\sim l_F$. However,

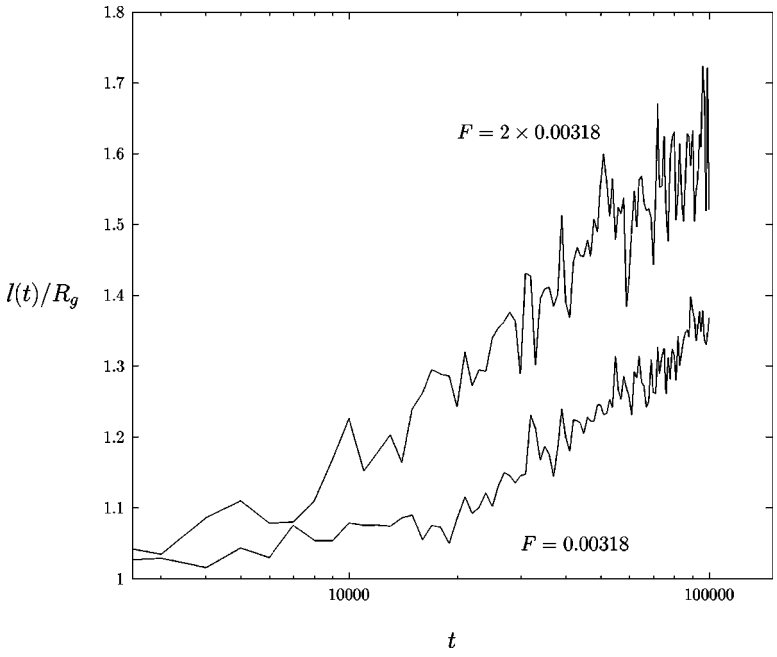

FIG. 7. Characteristic domain size as a function of time at $\epsilon=0.4$ and $F\neq0$ as indicated in the figure. The initial condition at time $t=0$ is a glassy configuration obtained from a previous run with $F=0$.

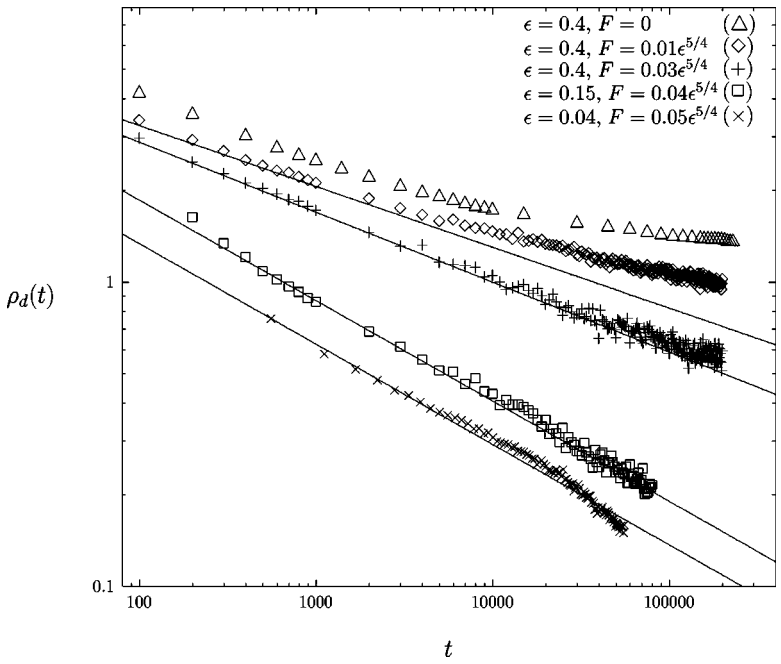

FIG. 8. Defect density in arbitrary units as a function of time for several values of ϵ and F. The straight solid lines are guides to the eye with slopes, from bottom to top, -0.33, -0.33, -0.23, and -0.20.

the effective initial decay is slower than $t^{-1/3}$, which we interpret as a crossover effect resulting from nonadiabaticity.

In summary, our results for large ϵ are in agreement with earlier numerical results performed at $\epsilon = 0.25$, showing that coarsening laws are very slow and depend on the presence of thermal fluctuations. We argue here that a coarsening exponent can be properly determined only in the small ϵ limit, where the phase ordering kinetics is self-similar. Our results support that the exponent $z = 3$ is independent of F for sufficiently small ϵ, when pinning effects are negligible (R_g much larger than the linear size of the system).

V. CONCLUSIONS

We have shown that the Swift-Hohenberg model of Rayleigh-Bénard convection exhibits glassy properties in spatially extended systems. In the absence of fluctuations, and following a parameter quench across threshold, random initial configurations do not evolve into completely ordered states, a single plane-wave or crystalline state. Instead, they reach disordered metastable configurations in which topological defects, mainly grain boundaries and disclinations, fail to annihilate and remain with finite density. It appears that the formation of these glassy configurations in a quenched disorder-free system can be accounted for by the finite separation between ''fast'' length scales of the structure (associated with stripe periodicity), and ''slow'' scales (associated with the extent of defect envelopes). Since at a finite distance from threshold the ratio between these two scales is finite, nonadiabatic effects lead systematically to defect pinning in an infinite system. Fluctuations allow unpinning and a certain amount of ''crystallization,'' albeit through an asymptotically slow activated motion of grain boundaries and other defects.

The present framework is far too simple to be used in the prediction of a glass transition temperature, if such a transition exists. In some respects, the situation just described is instead very similar to that of domain growth in random fields in dimension larger than two [44,45]. There, domain walls separating magnetized domains are pinned by fixed impurities and evolve by thermal activation to other more favorable configurations. The phenomenological pinning energy of a domain of size R grows as ΥR^{θ}, were θ depends on the problem considered, yielding an escape rate given by $r \sim \exp(-\Upsilon R^{\theta}/k_B T)$ equation that is formally analogous to Eq. (27) with $\theta = 1$. Two crucial differences are that our system is glassy even in two dimensions, and that defects do not need any disorder to become pinned.

The consequences of defect pinning on the intermediate time regime corresponding to domain coarsening have also been investigated. A universal coarsening exponent can be determined close to threshold only, where we obtain $z = 3$. Coarsening stops when the linear size of the system is larger than the characteristic domain size for pinning. In this situation, an intermediate crossover regime is anticipated with lower effective coarsening exponents, as is observed in numerical solutions of the model. Crossover effects induced by pinning can be reduced by either increasing the intensity of the fluctuations or approaching threshold.

We note that some of our conclusions as well as our interpretation of the numerical results are based on the analysis of a particular type of defect, namely, a grain boundary separating two domains with differently oriented stripes. We think it is likely that similar nonadiabatic corrections to defect motion will appear for dislocation glide or disclination motion, leading to similar nonperturbative corrections in ϵ to the speed of the defect.

We believe more generally that pinning through nonadiabatic effects is likely to be a feature of a wide variety of pattern forming systems, and is not limited to the particular model treated here. Block copolymer melts, for instance, provide an interesting case in which the results obtained could have practical implications (see Appendix A for a sum-

mary of the relevant equations and their relationship with the model studied here). We also mention here that results qualitatively similar to ours have been reported for a model with competing interactions (describing ferromagnetic films), that is, defined by the equations of Appendix A with a different form of the Green's function G [46]. There, frozen polycrystalline configurations of stripe patterns were observed for deep quenches as well, whereas the system could reach an ordered state for shallow quenches. This same model was also able to predict the formation of a frozen phase composed of polydisperse droplets with a near-hexagonal arrangement [47], as previously observed in experiments on a Langmuir monolayer [48]. However, the pinning mechanism involved in this last case is probably different than the one discussed in the present paper since the patterns are no longer locally periodic. Nevertheless, we would expect that our main conclusions can be readily extended to other systems with periodic structures such as hexagonal patterns [47,49].

ACKNOWLEDGMENT

This research has been supported by the U.S. Department of Energy, Contract No. DE-FG05-95ER14566.

APPENDIX A: MEAN-FIELD MODEL OF A SYMMETRIC BLOCK COPOLYMER MELT

We briefly recall in this appendix known results about the relationship between the mean-field description of a block copolymer melt, and the amplitude equation for Swift-Hohenberg model [Eq. (1)] at first order in ϵ. The dynamics of microphase separation of block copolymers is often modeled by a time-dependent Ginzburg-Landau equation for a conserved order parameter [35,50],

$$\frac{\partial \psi(\vec{r},t)}{\partial t} = M\nabla^2 \frac{\delta F}{\delta \psi(\vec{r},t)}, \tag{A1}$$

where

$$F = \int d\vec{r}\left(-\frac{r}{2}\psi^2 + \frac{u}{4}\psi^4 + \frac{K}{2}(\vec{\nabla}\psi)^2 \right) + \frac{B}{2}\int\int d\vec{r}\,d\vec{r}\,'\,\psi(\vec{r},t)G(\vec{r},\vec{r}\,')\psi(\vec{r}\,',t). \tag{A2}$$

G is the Green's function of the Laplacian operator $\nabla^2 G(\vec{r},\vec{r}\,') = -\delta(\vec{r}-\vec{r}\,')$ and M a constant mobility or Onsager coefficient. The scalar order parameter ψ is the local monomer concentration difference between the two chemical species. Following Ref. [51] we set $r = 2+\epsilon, u = 1, K = 1/k_0^2$, and $B = k_0^2$. Two independent parameters k_0 and (small) ϵ remain. Equation (A1) reduces to

$$\frac{1}{M}\frac{\partial \psi}{\partial t} = \nabla^2\left[-(2+\epsilon)\psi + \psi^3 - \frac{1}{k_0^2}\nabla^2\psi \right] - k_0^2(\psi - \psi_\infty), \tag{A3}$$

where ψ_∞ is the boundary condition at infinity. In most studies, it is customary to set $\psi_\infty = \langle \psi \rangle$, the spatial average of ψ over the sample. We introduce the amplitude A of slightly modulated waves through,

$$\psi(\vec{r},t) = \tfrac{1}{2}[A(\vec{r},t)e^{ik_0 x} + \text{c.c.}]. \tag{A4}$$

A multiscale analysis of Eq. (A3) in the limit $\epsilon \ll 1$ was conducted by Shiwa [51]. Setting $M = 1/k_0^2$, the resulting equation for the amplitude is

$$\frac{\partial A}{\partial t} = \epsilon A + \frac{4}{k_0^2}\left(\partial_x - \frac{i}{2k_0}\partial_y^2 \right)^2 A - \frac{3}{4}|A|^2 A, \tag{A5}$$

which is identical to the amplitude equation of the Swift-Hohenberg model. Note that the only effect of the conservation law on the local part of the free energy [the Laplacian operator in front of the square bracket in Eq. (A3)] is a renormalization of the mobility M. The quantities ϵ and k_0 defined above play the same role as the same coefficients in the Swift-Hohenberg model (i.e., the dimensionless distance to threshold and the dominant wave number of the structure, respectively).

APPENDIX B: CALCULATION OF THE DEFECT DENSITY IN THE PRESENCE OF FLUCTUATIONS

Computation of the domain size from the probability distribution of stripe curvature is delicate in the presence of noise. We have used a different method than that used for $F = 0$. We introduce an effective squared amplitude $\zeta(\vec{r},t)$ by

$$\zeta = \psi^2 + (\vec{\nabla}\psi)^2/k_0^2. \tag{B1}$$

For a perfectly ordered system consisting of a plane-wave solution of the Swift-Hohenberg equation and $F = 0$, the probability distribution function of ζ is a δ function at $\zeta_\infty = 4\epsilon/3$. When $F > 0$ the probability distribution function of ζ even for a plane wave $p_\infty^{(F)}(\zeta)$ is broader because of "phonon" excitations. The function $p_\infty^{(F)}$ is plotted in Fig. 6 (with dotted lines), and is then used as a reference curve for a fixed F. In a partially disordered configuration, the presence of defects and curved stripes further broadens the probability distribution function to $p^{(F)}(\zeta,t)$ (solid lines of Fig. 6). The difference between the two curves is related to the degree or disorder beyond small fluctuations away from a perfectly ordered structure. We define the defect density by $\rho_d(t) = \max\{p_\infty^{(F)}(\zeta),\zeta\} - \max\{p^{(F)}(\zeta,t),\zeta\}$. Since grain boundaries are seen to be the major contribution to defect density, one can introduce a characteristic length scale ρ_d^{-1}, which is further identified with the characteristic size, or domain size l. In Fig. 7, l has been normalized so that $l(t=0) = R_g$ (at the beginning of the heating process) where R_g is computed from the probability distribution function of stripe curvatures at $F = 0$.

[1] K. Kawasaki, Prog. Theor. Phys. Suppl. **79**, 161 (1984).
[2] H. Brand and K. Kawasaki, J. Phys. A **17**, L905 (1984).
[3] G. Mazenko, in *Formation and Interaction of Topological Defects*, edited by A.-C. Davis and R. Brandenberger (Plenum, New York, 1995).
[4] A. Bray, in *Formation and Interaction of Topological Defects* (Ref. [3]).
[5] I. Chuang, B. Yurke, A.N. Pargellis, and N. Turok, Phys. Rev. E **47**, 3343 (1993).
[6] H. Toyoki, Phys. Rev. E **47**, 2558 (1993).
[7] M. Zapotocky, P.M. Goldbart, and N. Goldenfeld, Phys. Rev. E **51**, 1216 (1995).
[8] N. Mason, A.N. Pargellis, and B. Yurke, Phys. Rev. Lett. **70**, 190 (1993).
[9] Y. Oono and M. Bahiana, Phys. Rev. Lett. **61**, 1109 (1988).
[10] K.R. Elder, J. Viñals, and M. Grant, Phys. Rev. Lett. **68**, 3024 (1992).
[11] K.R. Elder, J. Viñals, and M. Grant, Phys. Rev. A **46**, 7618 (1992).
[12] M.C. Cross and D.I. Meiron, Phys. Rev. Lett. **75**, 2152 (1995).
[13] Q. Hou, S. Sasa, and N. Goldenfeld, Physica A **239**, 219 (1997).
[14] J.J. Christensen and A.J. Bray, Phys. Rev. E **58**, 5364 (1998).
[15] D. Boyer and J. Viñals, Phys. Rev. E **64**, 050101 (2001).
[16] P. Manneville, *Dissipative Structures and Weak Turbulence* (Academic, New York, 1990).
[17] M. Cross and P. Hohenberg, Rev. Mod. Phys. **65**, 851 (1993).
[18] E.D. Siggia and A. Zippelius, Phys. Rev. A **24**, 1036 (1981).
[19] P. Manneville and Y. Pomeau, Philos. Mag. A **48**, 607 (1983).
[20] G. Tesauro and M. Cross, Philos. Mag. A **56**, 703 (1987).
[21] Y. Pomeau, Physica D **23**, 3 (1986).
[22] D. Bensimon, B. Shraiman, and V. Croquette, Phys. Rev. A **38**, 5461 (1988).
[23] B.A. Malomed, A.A. Nepomnyashchy, and M.I. Tribelsky, Phys. Rev. A **42**, 7244 (1990).
[24] M.-H. Julien *et al.*, Phys. Rev. Lett. **83**, 604 (1999).
[25] D. Kivelson *et al.*, Physica A **219**, 27 (1995).
[26] J. Schmalian and P.G. Wolynes, Phys. Rev. Lett. **85**, 836 (2000).
[27] M. Grousson, G. Tarjus, and P. Viot, Phys. Rev. Lett. **86**, 3455 (2001).
[28] J.D. Shore, M. Holzer, and J.P. Sethna, Phys. Rev. B **46**, 11 376 (1992).
[29] M.E.J. Newman and C. Moore, Phys. Rev. E **60**, 5068 (1999).
[30] C. Harrison *et al.*, Science **290**, 1558 (2000).
[31] L. Purvis and M. Dennin, Phys. Rev. Lett. **86**, 5898 (2001).
[32] J. Gunton, M. San Miguel, and P. Sahni, in *Kinetics of First Order Phase Transitions*, edited by C. Domb and J. Lebowitz, Phase Transitions and Critical Phenomena Vol. 8 (Academic, London, 1983).
[33] A. Bray, Adv. Phys. **43**, 357 (1994).
[34] J. Swift and P.C. Hohenberg, Phys. Rev. A **15**, 319 (1977).
[35] L. Leibler, Macromolecules **13**, 1602 (1980).
[36] D. Boyer and J. Viñals, Phys. Rev. E **63**, 061704 (2001).
[37] G. Ahlers, M. Cross, P. Hohenberg, and S. Safran, J. Fluid Mech. **110**, 297 (1981).
[38] P.C. Hohenberg and J.B. Swift, Phys. Rev. E **52**, 1828 (1995).
[39] J. Toner and D.R. Nelson, Phys. Rev. B **23**, 316 (1981).
[40] R. Graham, Phys. Rev. A **10**, 1762 (1974).
[41] F. Drolet and J. Viñals, Phys. Rev. E **57**, 5036 (1998).
[42] F. Drolet and J. Viñals, Phys. Rev. E **64**, 026120 (2001).
[43] F can be estimated to be of the order $F = u\epsilon^{5/4}$, with $u \leqslant 1$. See also Ref. [40].
[44] T. Natterman and J. Villain, Phase Transitions **11**, 5 (1988).
[45] J.-P. Bouchaud, L. Cugliandolo, J. Kurchan, and M. Mezard, in *Spin Glasses and Random Fields* (World Scientific, Singapore, 1998), p. 161.
[46] C. Sagui and R.C. Desai, Phys. Rev. E **49**, 2225 (1994).
[47] C. Sagui and R.C. Desai, Phys. Rev. E **52**, 2822 (1995).
[48] M. Seul, Europhys. Lett. **28**, 557 (1994).
[49] K.R. Elder, M. Katakowski, M. Haataja, and M. Grant, e-print cond-mat/0107381.
[50] T. Ohta and K. Kawasaki, Macromolecules **19**, 2621 (1986).
[51] Y. Shiwa, Phys. Lett. A **228**, 279 (1997).